Secretory leukocyte protease inhibitor influences periarticular joint inflammation in *B. burgdorferi*-infected mice

Qian Yu[1*], Xiaotian Tang[1,7], Thomas Hart[1], Robert Homer[2], Alexia A. Belperron[3], Linda K. Bockenstedt[3], Aaron Ring[4,5], Akira Nakamura[6], Erol Fikrig[1]

[1]Section of Infectious Diseases, Department of Internal Medicine, School of Medicine, Yale University, New Haven, Connecticut, USA. [2]Department of Pathology, School of Medicine, Yale University, New Haven, Connecticut, USA. [3] Section of Rheumatology, Allergy and Immunology, Department of Internal Medicine, School of Medicine, Yale University, New Haven, Connecticut, USA. [4]Department of Immunobiology, Yale School of Medicine, New Haven, CT, USA. [5]Department of Pharmacology, Yale School of Medicine, New Haven, CT, USA. [6]Divisions of Immunology, Faculty of Medicine, Tohoku Medical and Pharmaceutical University, Sendai, Japan.[7]Institute of Insect Sciences, College of Agriculture and Biotechnology, Zhejiang University, Hangzhou, China.

Corresponding authors:

Qian Yu, The Anlyan Center, 300 Cedar St. Rm 410, New Haven, CT, 06519, USA, (203)-843-8578, qian.yu@yale.edu

Authorship note: Qian Yu and Xiaotian Tang are co–first authors.

Conflict-of-interest: The authors have no conflicts of interest.

Abstract

Lyme disease, caused by *Borrelia burgdorferi*, is the most common tick-borne infection in the United States. Arthritis is a major clinical manifestation of infection, and synovial tissue damage has been attributed to the excessive pro-inflammatory responses. The secretory leukocyte protease inhibitor (SLPI) promotes tissue repair and exerts anti-inflammatory effects. The role of SLPI in the development of Lyme arthritis in C57BL/6 mice, which can be infected with *B. burgdorferi*, but only develop mild joint inflammation, was therefore examined. *SLPI*-deficient C57BL/6 mice challenged with *B. burgdorferi* had a higher infection load in the tibiotarsal joints and marked periarticular swelling, compared to infected wild type control mice. The ankle joint tissues of *B. burgdorferi*-infected *SLPI*-deficient mice contained significantly higher percentages of infiltrating neutrophils and macrophages. *B. burgdorferi*-infected *SLPI*-deficient mice also exhibited elevated serum levels of IL-6, neutrophil elastase, and MMP-8. Moreover, using a recently developed BASEHIT (**BA**cterial **S**election to **E**lucidate **H**ost-microbe **I**nteractions in high **T**hroughput) library, we found that SLPI directly interacts with *B. burgdorferi*. These data demonstrate the importance of SLPI in suppressing periarticular joint inflammation in Lyme disease.

43 **Introduction**

44

45 Lyme disease is the most common tick-borne illness in the United States,
46 affecting an estimated 500,000 people each year[1]. The spirochete *Borrelia burgdorferi* is
47 the causative agent of Lyme disease and is primarily transmitted by *Ixodes scapularis*
48 ticks in North America[2]. Early administration of antibiotics is usually successful in the
49 treatment of Lyme disease. However, between 2008-2015, arthritis was the major
50 manifestation in a third of Lyme disease cases reported to CDC[3,4]. Musculoskeletal
51 symptoms occur at all stages of Lyme disease, with migratory arthralgias in the early
52 stages and frank arthritis occurring months later. Lyme arthritis can present as acute or
53 intermittent self-resolving episodes or persistent joint swelling and pain, which if left
54 untreated, can lead to irreversible joint dysfunction and debilitation[3,5,6]. Although Lyme
55 arthritis resolves completely with antibiotic therapy in most patients, a small percentage
56 of individuals experience persistent joint inflammation for months or several years,
57 termed post-infectious Lyme arthritis[3,5,7].

58

59 Studies of synovial fluid from Lyme arthritis patients found infiltrating
60 polymorphonuclear cells (PMNs), IFN-γ-producing mononuclear cells, and large
61 amounts of NF-κB-induced pro-inflammatory cytokines and chemokines, such as IL-6,
62 CXCL10, and TNF-α[6,8-10]. An inverse correlation between the robust IFN-γ signature
63 and tissue repair has been demonstrated in the synovial tissue and fluid from patients
64 with post-infectious Lyme arthritis[11]. This suggests that the dysregulated excessive pro-
65 inflammatory responses inhibit tissue repair and lead to extensive tissue damage.

66

67 *B. burgdorferi* infection of laboratory mice causes an acute arthritis, the severity
68 of which is mouse strain dependent[12]. *B. burgdorferi* infected-C3H/HeN mice develop
69 pronounced neutrophilic infiltration of periarticular structures and the synovial lining
70 which peaks in severity several weeks after infection[13]. In contrast, infection of *B.*
71 *burgdorferi* C57BL/6 mice causes mild, if any, arthritis[14]. On a C57BL/6 background, the
72 immune-deficient RAG-/- and SCID mice are also resistant to *B. burgdorferi*-induced
73 arthritis, indicating that responses independent of humoral and cellular immunity
74 contribute to the milder phenotype of disease in these animals[15]. Similar to Lyme
75 arthritis in humans, neutrophils, macrophages, and signaling involving IFN-γ and NF-κB
76 contribute to the severity of murine joint inflammation[16-19].

77

78 The secretory leukocyte protease inhibitor (SLPI) is a 12 kDa, secreted, non-
79 glycosylated, cysteine-rich protein[20]. It strongly inhibits serine proteases, especially
80 neutrophil-derived serine proteases (NSPs) including cathepsin G (CTSG) and elastase
81 (NE)[21,22]. It is secreted by epithelial cells at various mucosal surfaces and is also
82 produced by neutrophils, macrophages, mast cells, and fibroblasts[23,24]. The major
83 function of SLPI is to inhibit excessive protease activity at sites of inflammation, thus
84 promoting tissue repair and wound healing[25,26]. SLPI also exerts anti-inflammatory
85 function by inhibiting NF-κB activation in macrophages[27-29]. The roles of neutrophils and
86 NSPs have been extensively studied in rheumatoid arthritis, a condition sharing some
87 similarities with Lyme arthritis[30,31]. NE and CTSG induce potent destruction of cartilage
88 proteoglycan *in vitro* and *in vivo*, which contributes to rheumatoid arthritis progression[32].

Some studies also demonstrated that SLPI inhibits joint inflammation and bone destruction[33,34]. However, the importance of SLPI and NSPs have not been studied in the context of Lyme disease.

Thus, in this study, we examined the role of SLPI in the development of murine Lyme arthritis caused by *B. burgdorferi*. Using the *SLPI*-deficient C57BL/6 mice, we observed a significant increase in the infection burden and marked periarticular swelling in the ankle joints compared to WT mice following *B. burgdorferi* infection. Significant increase in infiltrating neutrophils and macrophages were observed in the ankle joints of infected *SLPI*-deficient mice. Elevated serum levels of IL-6, neutrophil elastase, and MMP-8 in the infected *SLPI*-deficient mice were also observed, which can lead to the recruitment of neutrophils and macrophages exacerbating the periarticular swelling. We further demonstrated the direct interaction between SLPI and *B. burgdorferi*. This is the first study showing the importance of anti-protease-protease balance in the development of murine Lyme arthritis.

105 **Results**

106

107 ***Secretory leukocyte protease inhibitor (SLPI) influences periarticular joint***
108 ***inflammation in B. burgdorferi-infected mice.***

109

110 To assess the importance of SLPI during murine Lyme arthritis, we compared the
111 outcomes of *B. burgdorfe*ri infection of C57BL/6 WT and *SLPI*-/- mice. The C57BL/6 WT
112 and *SLPI*-/- mice were infected with 10^5 spirochetes subcutaneously. Infection burdens
113 in the skin were assessed by qPCR of *B. burgdorferi* DNA in ear punch biopsies at 7,
114 14, and between 21 to 24 dpi (Figure 1, A-C). Infection burdens in the heart (Figure 1D)
115 and tibiotarsal joint (Figure 1E) tissues were assessed between 21 to 24 dpi. We did not
116 observe any significant difference in infection burden in the skin between WT and *SLPI*-
117 /- mice (n=24) at 7, 14, 21 to 24 dpi, or in the heart between 21 to 24 dpi (Figure 1, A-
118 D).

119

120 Strikingly, we observed a significantly higher spirochete burden in the ankle joints
121 of infected *SLPI*-/- mice (n=24) between 21 to 24 dpi (Figure 1E). Furthermore, at
122 around 24 dpi, significant swelling was also observed solely in the infected *SLPI*-/- mice
123 (Figure 2A, red arrow). The level of swelling was first scored visually. While 14 out of 20
124 infected *SLPI*-/- mice displayed visible swelling (score ≥ 1), only 1 in 14 infected WT
125 mice displayed mild swelling (score 1) at the ankle (Figure 2B). The tibiotarsal joints
126 were then dissected, fixed, and stained with H&E for histopathological evaluation of the
127 level of inflammation (Figure 2, C and D). Inflammation of bursa and soft tissue adjacent

128 to the tibiotarsal joint, but not in the tibiotarsal synovium, was consistently observed in
129 the infected *SLPI*-/- mice (Figure 2C, black rectangle). In contrast, only 1 out of 14
130 infected WT mice displayed modest inflammation (score = 2) in these sites (Figure 2D).
131 The above data indicate the importance of SLPI in modulating the development of
132 periarticular inflammation associated with murine Lyme arthritis.
133
134 ***SLPI influences immune responses in B. burgdorferi-infected mice.***
135
136 It has been established that SLPI exerts its anti-inflammatory effect by inhibiting
137 neutrophil serine protease and by dampening NF-κB activation in macrophages[22]. Thus,
138 to investigate the mechanism underlying the effect of SLPI on murine joint inflammation,
139 we sought to identify the population of infiltrating cells in the periarticular tissues of
140 infected WT and *SLPI*-/- mice. Between 21 to 24 dpi, the ankle joints were dissected. To
141 obtain single cell suspensions of infiltrating cells, bone marrow cells were removed and
142 discarded and the joint and periarticular tissues were digested[35]. The cells were stained
143 for flow cytometry with CD45, CD11b, and LY6G to label neutrophils (Figure 3A), and
144 CX3CR1, CD64, and LY6C to label macrophages (Figure 3B)[36]. After gating, we
145 observed significantly higher percentages of infiltrating neutrophils and macrophages in
146 the dissected tissues from infected *SLPI*-/- than WT mice (Figure 3, A and B). To further
147 eliminate the possibility of neutrophilic contamination within the macrophage population,
148 we also implemented a Ly6G-negative gating strategy. The result showed a consistently
149 higher percentage of macrophages in the infected *SLPI*-/- mice (Supplemental Figure
150 1). Using RT-qPCR on the tibiotarsal tissues extracted from *B. burgdorferi*-infected

151 *SLPI*-/- mice, we detected increased gene expression of neutrophil chemoattractant
152 receptor C-X-C motif chemokine receptor 2 (*CXCR2)*, monocyte chemoattractant
153 protein 1 (*MCP-1*), and its receptor C-C motif chemokine receptor 2 (*CCR2)* (Figure 3,
154 C-E).
155
156 Furthermore, the serum cytokine/chemokine profile was assessed from
157 uninfected and *B. burgdorferi*-infected WT and *SLPI*-/- mice between 21 to 24 dpi. We
158 observed a significant increase in IL-6 in infected *SLPI*-/- mice (Figure 3F). IL-6 recruits
159 and stimulates neutrophils, leading to secretion of neutrophil-derived serine proteases
160 including neutrophil elastase (NE) and cathepsin G (CTSG)[37]. The lack of serine
161 protease inhibitors, such as SLPI, can cause excessive protease activity and
162 subsequent tissue damage and inflammation[31]. Indeed, using ELISA, we observed a
163 significantly higher level of NE solely in the serum of infected *SLPI*-/- mice (Figure 3G).
164 An increased serum level of NE was also observed in the *B. burgdorferi*-infected,
165 arthritis-susceptible C3H/HeN mice at 21 dpi (Figure 3H). These data suggest that, in
166 the absence of SLPI, excessive serine protease activity can exacerbate murine Lyme
167 arthritis.
168
169 A correlation between IL-6, macrophages, metalloproteinases (MMPs), and
170 articular cartilage destruction has been observed in the synovial tissue of RA patients[38].
171 Elevated levels of host matrix metalloproteinases (MMPs) have also been found in the
172 synovial fluid of Lyme arthritis patients and can cause excessive tissue damage[39]. Thus,
173 a mouse MMP 5-Plex Discovery Assay was used to explore the serum levels of different

174 MMPs. We observed a significant increase in the levels of MMP-8 solely in the infected
175 *SLPI*-/- mice (Figure 3I). Taken together, our data suggest that SLPI suppresses
176 inflammation in *B. burgdorferi*-infected mouse joint tissues by potentially inhibiting
177 neutrophil and macrophage infiltration and subsequent protease-mediated tissue
178 destruction.
179
180 ***Decreased serum level of SLPI in Lyme disease patients.***
181
182 Despite numerous studies of serum, synovial fluid and tissue from Lyme arthritis
183 patients, the importance of anti-protease-protease balance in Lyme arthritis has not
184 been investigated[7]. Based on our data obtained from the *SLPI*-deficient mice, we
185 assessed the serum SLPI level in Lyme disease patients (Figure 4). Due to the limited
186 samples available from Lyme arthritis patients, we included samples from Lyme disease
187 patients who presented with earlier manifestations of Lyme disease. The serum level of
188 human SLPI assessed by ELISA showed a significant decrease in the SLPI level in
189 Lyme disease patients comparing to healthy adult controls (Figure 4). Similar to our data
190 from *B. burgdorferi*-infected mice, this result suggests a correlation between the lack of
191 SLPI and humans exhibiting clinical manifestations of Lyme disease, including arthritis.
192
193 ***SLPI interacts with B. burgdorferi.***
194
195 It has been demonstrated that *B. burgdorferi* interacts with various mammalian
196 proteins to establish infection in the mammalian host[40-43]. Thus, we postulated that *B.*

197 *burgdorferi* could interact with SLPI to influence the progression of joint inflammation. To
198 test this hypothesis, we probed a recently developed BASEHIT (**BA**cterial **S**election to
199 **E**lucidate **H**ost-microbe **I**nteractions in high **T**hroughput) library with *B. burgdorferi*[40,44-
200 46]. BASEHIT utilizes a genetically barcoded yeast display library expressing 3,324
201 human exoproteins, thus enabling a comprehensive screen of host-microbe interactions
202 in a high-throughput fashion. Human SLPI is one of the exoproteins that passed the
203 significance threshold, indicating *B. burgdorferi*-SLPI binding. To further establish that
204 hSLPI directly binds to *B. burgdorferi*, we performed ELISA with whole cell *B.*
205 *burgdorferi* lysates. We observed strong binding between whole cell *B. burgdorferi*
206 lysates and hSLPI at a level as low as 10 nM (Figure 5A).
207
208 To extend these studies, flow cytometry was performed using intact *B.*
209 *burgdorferi* and both human and murine SLPI. A significant increase in fluorescence
210 intensity was observed when *B. burgdorferi*, cultivated at 33°C, was incubated with
211 human SLPI at 10 nM and 1 μM level (Figure 5B). Though the binding to 10 nM rmSLPI
212 was at background level, we observed a significant increase in fluorescence intensity
213 when *B. burgdorferi* were incubated with 1 μM rmSLPI (Figure 5C). Flow cytometry also
214 demonstrated increased binding of *B. burgdorferi* cultured at 37 °C to 1 μM hSLPI or
215 rmSLPI (Figure 5, B and C). This indicates that the binding was more robust when
216 performed at temperatures that *B. burgdorferi* encounter in the mammalian host.
217 Immuno-fluorescent microscopy was an additional method that also demonstrated direct
218 binding of *B. burgdorferi* with human or murine SLPI (Figure 5D).
219

220 In contrast to *B. burgdorferi* B31-A3, an infectious strain used throughout this
221 study, we did not observe any binding between hSLPI and *B. burgdorferi* B31A, a high-
222 passage non-infectious strain (Supplemental Figure 2A)[47,48]. The above observation
223 further suggests that the direct interaction between SLPI and *B. burgdorferi* could
224 impact the pathogenesis of murine Lyme arthritis. To further investigate the potential *B.*
225 *burgdorferi* ligand that interacts with SLPI, we probed protease-treated *B. burgdorferi*
226 lysates with hSLPI using ELISA. After treatment with proteinase K, we observed a
227 marked decrease in binding of hSLPI to *B. burgdorferi* lysates (Supplemental Figure
228 2B). This result suggests that hSLPI can directly interact with a *B. burgdorferi* protein.
229
230 It has been showed that SLPI has antimicrobial effects against multiple gram-
231 negative and positive bacteria[49-51]. However, using the BacTiter-Glow microbial cell
232 viability assay, we did not observe any significant changes in *B. burgdorferi* viability in
233 the presence of hSLPI (Supplemental Figure 3A). A previous study also demonstrated
234 that the tick salivary protein, Salp15, specifically interacted with *B. burgdorferi* outer
235 surface protein C (OspC)[52]. The binding of Salp15 protected spirochetes from killing by
236 polyclonal mouse or rabbit antisera *in vitro*[52,53]. However, again, using the BacTiter-
237 Glow microbial cell viability assay, the pre-incubation of hSLPI did not protect
238 spirochetes from killing by mouse *B. burgdorferi* antisera (Supplemental Figure 3B).
239 Thus, the importance of the SLPI-*B. burgdorferi* interaction and the direct effect of such
240 an interaction on *B. burgdorferi* biology is likely independent of direct borreliacidal
241 activity or any interference with the antibody-mediated *B. burgdorferi* killing.
242

243 **Discussion**

244

245 Lyme arthritis has been extensively documented and studied in patients and *B.*
246 *burgdorferi*-infected mice. The pathogenesis of Lyme arthritis is characterized by
247 synovial tissue damage caused by infiltration of immune cells and excessive pro-
248 inflammatory responses[7]. Transcriptomic studies also revealed the suppression of
249 tissue repair genes in the synovial tissue of Lyme arthritis patients and tibiotarsal joint
250 tissues of *B. burgdorferi*-infected mice[11,54]. However, the roles of the genes involved in
251 tissue repair have not been studied.

252

253 SLPI strongly inhibits serine proteases, especially cathepsin G and elastase
254 secreted by neutrophils[20]. The major function of SLPI is to prevent unnecessary tissue
255 damage caused by excessive protease activity, thus promoting tissue repair and
256 homeostasis[55]. The lack of SLPI impairs wound healing and tissue repair [25] and SLPI
257 also inhibits NF-κB activation and downstream pro-inflammatory cytokine release from
258 macrophages[27,29]. Thus, we hypothesized that SLPI plays an important role in Lyme
259 arthritis. To test this hypothesis, we employed *SLPI*-/- C57BL/6 mice. As C57BL/6 mice
260 only develop mild arthritis, if any, after challenge with *B. burgdorferi*, this mouse
261 provided an ideal example to study whether the lack of SLPI could cause an arthritis-
262 resistant mouse to become arthritis-susceptible. Compared to WT C57BL/6 mice, *B.*
263 *burgdorferi* infection in the *SLPI*-/- mice consistently showed a significantly higher
264 infection burden in tissues extracted from the ankle joint, which included periarticular
265 structures (Figure 1E). Severe swelling and inflammation in the bursal and soft tissue

266 around tibiotarsal joints were observed solely in the infected *SLPI*-/- mice (Figure 2).
267 The significant increase in the infection burden in *SLPI*-/- mice can contribute to the
268 enhanced periarticular inflammation following *B. burgdorferi* infection. However, these
269 data also emphasize the importance of SLPI in controlling the development of
270 inflammation in periarticular tissues of *B. burgdorferi*-infected mice. Indeed, in a
271 *Streptococcal* cell wall (SCW)-induced arthritis model in rats, the intraperitoneal
272 injection of SLPI significantly decreased the severity of joint swelling[34]. Targeting the
273 SLPI-associated anti-protease pathways could also potentially be a strategy for
274 ameliorating periarticular inflammation that occurs in some rheumatic diseases.
275
276 Analysis of *B. burgdorferi* infection in the *SLPI*-/- and WT mice revealed a
277 significant increase in infiltrating neutrophils and macrophages in the periarticular
278 tissues of *SLPI*-/- mice (Figure 3, A and B). This observation is consistent with clinical
279 studies that showed a high percentage of neutrophils in the synovial fluid during active
280 infection[56,57]. In post-treatment Lyme arthritis, fewer neutrophils and more macrophages
281 are present in patients' synovial fluid[7]. In arthritis-susceptible C3H/He mice, *B.*
282 *burgdorferi* infection also leads to neutrophil infiltration in the periarticular tissues as well
283 as in the synovium of ankle joints[13]. The neutrophil chemoattractant KC (CXCL1) and
284 receptor CXCR2 mediates neutrophil recruitment and is critical for the development of
285 murine Lyme arthritis. Both *KC*-/- and *CXCR2*-/- C3H mice developed significantly less
286 ankle swelling when infected with *B. burgdorferi*[16,18]. Consistently, we observed a
287 significant increase in CXCR2 gene expression in the tibiotarsal joint tissues (Figure
288 3C), which can recruit neutrophils and cause more severe inflammatory soft tissue

289 infiltrates in the *SLPI*-/- mice. Monocyte chemoattractant protein-1 (MCP-1/CCL2) and
290 receptor CCR2 contribute to macrophage infiltration[58]. Though little to no difference in
291 arthritis was observed in the CCR2-/- mice, a high level of MCP-1 was detected in the
292 tibiotarsal tissues of *B. burgdorferi*-infected, arthritis-susceptible C3H/He mice,
293 suggesting a function for macrophages[18]. In the infected *SLPI*-/- mice, a significant
294 increase in both MCP-1 and CCR2 gene expression was observed in the tibiotarsal
295 tissues (Figure 3, D and E). Our data suggest that both neutrophils and macrophages
296 contribute to the severe periarticular inflammation in the infected *B. burgdorferi*-infected
297 *SLPI*-/- mice.
298
299 To investigate the underlying mechanism whereby SLPI deficiency enhanced
300 periarticular joint inflammation, we examined the serum cytokine/chemokine profile of *B.*
301 *burgdorferi*-infected *SLPI*-/- and WT mice. There was a significant increase in IL-6 solely
302 in the infected *SLPI*-/- mice (Figure 3F). An elevated IL-6 level has been demonstrated
303 in the serum, synovial fluid, and synovial tissue from Lyme arthritis patients[9,56]. IL-6 is
304 also pivotal in the pathogenesis of rheumatoid arthritis and correlates with the disease
305 severity and joint destruction[37]. It has been shown that IL-6 recruited neutrophils in an *in*
306 *vitro* co-culture rheumatoid arthritis model[59]. Neutrophils can be activated by IL-6
307 through binding of IL-6 receptor (IL-6R)[37]. Activated neutrophils release several
308 neutrophil serine proteases (NSPs) including neutrophil elastase (NE), cathepsin G
309 (CTSG), and proteinase-3 (PR3), which can lead to potent cartilage destruction[31].
310 Indeed, we observed a significant increase in the NE level in the serum of *B.*
311 *burgdorferi*-infected *SLPI*-/- but not WT mice (Figure 3G). In the arthritis susceptible

312 C3H/HeN mice, *B. burgdorferi* infection also induced a significant increase in the serum
313 NE level (Figure 3H). Interestingly, despite the known function of TNF-α in inflammatory
314 responses, we did not observe any significant changes in either TNF-α serum protein
315 levels or TNF-α gene expression levels in the *B. burgdorferi*-infected *SLPI*-/- and WT
316 mice (Supplemental Figure 4). The result is consistent with previous microarray data
317 that did not show significant changes in TNF-α levels in the C57BL/6 mice following *B.*
318 *burgdorferi* infection[54]. The above data indicate that the excessive serum neutrophil
319 elastase contributed to the periarticular inflammation in the *B. burgdorferi*-infected *SLPI*-
320 /- mice.
321
322 Matrix metalloproteinases (MMPs) target extracellular matrix and cause articular
323 cartilage destruction[60]. A correlation between IL-6 and MMPs expression has been
324 reported in the context of rheumatoid arthritis[38,61]. Elevated levels of several MMPs
325 have also been found in the synovial fluid of Lyme arthritis patients[39]. Thus, we also
326 investigated the MMPs profile in the *B. burgdorferi*-infected *SLPI*-/- and WT mice. We
327 observed a significant increase in the serum level of MMP-8 in the infected *SLPI*-/- mice
328 (Figure 3I). MMP-8 is known as neutrophil collagenase[62]. Using synovial fluid samples,
329 it has been reported that the level of MMP-8 was significantly higher in the patients with
330 post infectious Lyme arthritis than patients with active infection[63]. A comprehensive
331 examination of the MMP profile in the synovial fluid of patients with Lyme arthritis
332 revealed elevated levels of MMP-1, -3, -13, and -19[64]. *B. burgdorferi* infection induced
333 MMP-3 and MMP-19 in the C3H/HeN mice but not in the Lyme arthritis-resistant
334 C57BL/6 mice[64]. The differences in the MMP profiles provide an explanation for the

335 differences between human and murine Lyme arthritis. This finding further emphasizes
336 that excessive protease activity can contribute to the severity of periarticular
337 inflammation in *B. burgdorferi*-infected mice.
338
339 Previous research using serum, synovial fluid and tissue from Lyme arthritis
340 patients has been heavily focusing on innate and adaptive immune responses[7]. As a
341 result, limited data can be found regarding anti-protease and protease responses during
342 Lyme arthritis in human patients. In this study, we tested serum SLPI level in 5 healthy
343 subjects, 8 Lyme disease patients, 3 of whom had overt arthritis. Though the number of
344 healthy subjects is small, the median level of SLPI tested here (38.92 ng/ml, Figure 4) is
345 comparable with previous studies showing in average about 40 ng/ml SLPI in the serum
346 from healthy volunteers [65,66]. While the clinical manifestation of 5 of the patients with
347 Lyme disease was an EM skin lesion (Supplemental Table 1), some symptom persisted
348 several months after diagnosis, a timeframe when acute arthritis often develops. We
349 observed decreased SLPI in the serum of these patients (Figure 4), suggesting an
350 inverse relationship between the SLPI level and *B. burgdorferi*-infection. However, a
351 large number of sera and synovial fluid samples from patients with Lyme arthritis and
352 other clinical manifestations of Lyme disease are needed to establish a definitive
353 association.
354
355 *B. burgdorferi* first infects the skin of a vertebrate host following a tick bite, then
356 disseminates throughout the body, colonizes various tissue, evades immune responses,
357 and persists for a significant period of time. To survive the above processes, *B.*

358 *burgdorferi* interacts with various mammalian proteins, including decorin[41], fibronectin[42],
359 and plasminogen[43], among others. To comprehensively study the potential interaction
360 between *B. burgdorferi* and the host, our lab employed the BASEHIT (**BA**cterial
361 **S**election to **E**lucidate **H**ost-microbe **I**nteractions in high **T**hroughput) to assess the
362 interactions between *B. burgdorferi* and 3,336 human extracellular and secreted
363 proteins[44,46]. Using BASEHIT, our lab previously identified a strong interaction between
364 *B. burgdorferi* and Peptidoglycan Recognition Protein 1 (PGYRP1)[40]. Increased
365 infection burden in the heart and joint was observed in the mice lacking PGYRP1,
366 suggesting a role of PGYRP1 in the host response to *B. burgdorferi* infection.
367 Expanding the use of BASEHIT, CD55 was identified to bind *Borrelia crocidurae* and
368 *Borrelia persica*, two pathogens causing relapsing fever[45]. CD55-deficient mice infected
369 with *B. crocidurae* displayed lower pathogen load and elevated pro-inflammatory
370 cytokines. The above data demonstrate BASEHIT as an effective method to identify
371 host factors important in *B. burgdorferi* pathogenesis *in vivo*. In this study, we identified
372 an interaction between SLPI and *B. burgdorferi* using BASEHIT library screening and
373 subsequent flow cytometric analysis (Figure 5). The antimicrobial activity of SLPI has
374 been demonstrated against both gram-negative and positive bacteria including
375 *Escherichia coli*, *Pseudomonas aeruginosa*[49], *Mycobacteria tuberculosis*[50],
376 *Staphylococcus aureus*[51], and *Staphylococcus epidermidis*[49]. Interaction between the
377 positive charges of SLPI and the negative charges of bacteria surface, including
378 lipopolysaccharide (LPS), can destabilize bacteria cell wall leading to the bactericidal
379 effect[67]. *B. burgdorferi* do not have LPS[68] and this may account for the absence of the
380 bactericidal effect of SLPI against *B. burgdorferi* (Supplemental Figure 3A). Future

381 research is needed to understand the significance of the SLPI-*B. burgdorferi* binding in
382 the development of periarticular inflammation. The potential *B. burgdorferi* protein that
383 interact with SLPI remains unknown. It is our hypothesis that SLPI may bind and inhibit
384 an unknown *B. burgdorferi* virulence factor that could contribute to the development of
385 murine Lyme arthritis.
386
387 In conclusion, our data demonstrated the importance of SLPI in suppressing *B.*
388 *burgdorferi*-induced periarticular inflammation in mice by inhibiting recruitment of
389 neutrophils and macrophages and subsequent protease levels. We propose that, during
390 the active infection of the murine joint structures, the binding of *B. burgdorferi* with SLPI
391 depletes the local environment of SLPI. Such binding is specific to the infectious strain
392 of *B. burgdorferi.* As a potent anti-protease, the decrease in SLPI results in excessive
393 protease activity, including neutrophil elastase and MMP-8. These unchecked proteases
394 can lead to extensive tissue inflammation. Our study is the first to emphasize the
395 importance of an anti-protease-protease balance in the development of the periarticular
396 inflammation seen in *B. burgdorferi*-infected mice.
397

398 **Materials and methods**

399

400 **Sex as a biological variable**

401 Females *SLPI*-/- and WT C57BL/6 mice were used for the *in vivo B. burgdorferi*
402 infection. We have examined *B. burgdorferi* infection in both male and female C57BL/6
403 mice and no differences in the development of infection or disease have been noted.
404 Both male and female Lyme disease patients were included in the study. Sex was not
405 considered as a biological variable.

406

407 **Study approval**

408 This study used archived serum samples from adult Lyme disease subjects and
409 healthy controls that were previously collected under NIH U19AI089992 with approval of
410 the Yale University Institutional Review Board for human subjects research (IRB
411 protocol# 1112009475). All the animal experiments in this study were performed in
412 accordance with the Guidelines for the Care and Use of Laboratory Animals of the
413 National Institutes of Health. The animal protocols were approved by the Institutional
414 Animal Care and Use Committee at the Yale University School of Medicine.

415

416 **Measurement of serum SLPI levels in Lyme disease subjects and controls**

417 SLPI levels were measured in a total of 23 serum samples from 7 subjects at the
418 time of Lyme disease diagnosis (4 with a single erythema migrans lesion and 3 with the
419 late manifestation of Lyme arthritis) and from 5 healthy controls. Serum samples from
420 Lyme disease subjects were available at up to 3 times points: 1) study entry, range 0-9

421 days after onset of symptoms, 2) 30 days post diagnosis, and 3) up to 3 months after
422 completion of antibiotic therapy (range 4.5 – 6 months after dx). Additional details can
423 be found in Supplemental Table 1. The level of SLPI in the serum was measured using
424 the Human SLPI DuoSet ELISA kit (R&D Systems, #DY1274-05).
425
426 ***B. burgdorferi* culture**
427 *B. burgdorferi* B31-A3, an infectious clonal derivative of the sequenced strain
428 B31, was a generous gift from Dr. Utpal Pal at the Department of Veterinary Medicine,
429 University of Maryland, College Park[69]. *B. burgdorferi* B31-A3 and *B. burgdorferi* B31A
430 was grown in Barbour-Stoenner-Kelly H (BSK-H) complete medium (Sigma-Aldrich,
431 #B8291) in a 33°C setting incubator. The live cell density was determined by dark field
432 microscopy and using a hemocytometer (INCYTO, #DHC-N01). Low passage (P<3) *B.*
433 *burgdorferi* B31-A3 was used throughout this study.
434
435 ***In vivo* infection of mice**
436 The *SLPI*-/- C57BL/6 mice have been described previously[70,71]. The wild-type
437 (WT) C57BL/6 mice were purchased from the Jackson Laboratory and used as the
438 controls. 5 to 7 weeks of age female WT and *SLPI*-/- C57BL/6 mice were used for
439 infection. 4 to 6 weeks of age female C3H/HeN mice were purchased from Charles
440 River Laboratories and used for infection. Both C57BL/6 and C3H/HeN mice were
441 infected with low passage 10^5 *B. burgdorferi* subcutaneously (5–9 mice/group). PBS
442 sham-infected mice were used as controls. Mice were euthanized approximately 3-week
443 post infection within a 3-day window (between 21 to 24 dpi) based on the feasibility and

444 logistics of the laboratory. Ear punch biopsies were taken at 7-, 14- and between 21 to
445 24-day post-infection (dpi) to determine the infection burden in the skin. Between 21 to
446 24 dpi, mice were euthanized, and heart and joint tissues were collected to quantify the
447 spirochete burden. The protocol for the use of mice was reviewed and approved by the
448 Yale Animal Care and Use Committee.
449
450 **Quantification of *Borrelia* burden**
451 DNA was extracted from heart, tibiotarsal joint, and ear punch samples using
452 Qiagen DNeasy Blood & Tissue Kit, Qiagen. Quantitative PCR was performed using iQ-
453 SYBR Green Supermix (Bio-Rad). For quantitative detection of *B. burgdorferi* burden
454 within mouse tissue samples, q-PCR was performed with DNA using flagellin (*flaB*), a
455 marker gene for *Borrelia* detection. The mouse *β-actin* gene was used to normalize the
456 amount of DNA in each sample. The nucleotides sequences of primers used in specific
457 PCR applications are described previously[40].
458
459 **Joint histopathology analysis**
460 Mice were euthanized by CO_2 asphyxiation and one rear leg from each mouse
461 were dissected, immersion-fixed in Bouin's solution (Sigma-Aldrich, #HT10132). Fixed
462 tissues were embedded, sectioned, and stained with hematoxylin and eosin (HE) by
463 routine methods (Comparative Pathology Research Core in the Department of
464 Comparative Medicine, Yale School of Medicine). Periarticular and joint inflammation
465 was scored in a blinded fashion in a graded manner from 0 (negative), 1 (minimal), 2
466 (moderate), to 3 (severe).

467

468 **Flow cytometry to quantify infiltrating cells in joint tissues in mice**

469 The WT and *SLPI*-/- C57BL/6 mice were infected with *B. burgdorferi* as described
470 above. The mice were euthanized between 21 to 24 dpi. The ankle joints were cut out at
471 around 0.7 cm proximal to the ankle joint. The portion distal to the midfoot was
472 discarded, and the skin removed. The bone marrow cells were flushed out with RPMI
473 1640 (Gibco, #11875-093) using a 27-gauge needle. The bone marrow-depleted ankles
474 were cut into 3-4 mm sized tissue pieces and incubated with digestion media containing
475 2.4 mg/ml hyaluronidase (Sigma-Aldrich, #H3506), 1 mg/ml collagenase (Sigma-Aldrich,
476 #C2139) in RPMI 1640 (Gibco, #11875-093) supplemented with 10% fetal bovine serum
477 (FBS) for 1 h at 37 °C with 5%CO_2. The digestion media containing the tissue pieces
478 were passed through a 70 µm cell strainer (Thermo Scientific, #352350). The remaining
479 tissue pieces were mashed using a 10 ml syringe plunger. The digestion media
480 containing the isolated cells were neutralized with RPMI 1640 with 10% FBS[35]. The red
481 blood cells were lysed by ACK Lysing buffer (Gibco, #A1049201). The cells were rinsed
482 and resuspended in FACS buffer and ready for staining for flow cytometry.

483

484 The cells were incubated with Fc receptor antibody (TruStain FcXTM anti-mouse
485 CD16/32) (BioLegend, #101320), and antibodies including PerCP anti-mouse CD45
486 (BioLegend, #103130), BV711 anti-mouse Ly6G (BioLegend, #127643), PE anti-mouse
487 CD11b (BioLegend, #101208), APC/CY7 anti-mouse CX3CR21 (BioLegend, #149047),
488 FITC anti-mouse Ly6C (BioLegend, #128005), APC anti-mouse CD64 (BioLegend,
489 #139305) and LIVE/DEADTM fixable violet stain kit (Invitrogen, #L34955) on ice for 30

490 min. The samples were rinsed twice with FACS buffer and run through BD LSRII (BD
491 bioscience). The data was then analyzed by FlowJo[36].
492
493 **Gene expression evaluation by quantitative real-time PCR**
494 Mice were euthanized between 21 to 24 dpi. The ankle joints were excised as
495 described above, snap-frozen in liquid nitrogen, and stored at −80°C. The frozen tissue
496 was pulverized in liquid nitrogen using a mortar and pestle[72]. The RNA was purified
497 using Trizol (Invitrogen, #15596-018) following a published protocol[73]. cDNA was
498 synthesized using the iScript cDNA Synthesis Kits (Bio-Rad, #1708891). qPCR was
499 performed using iQ SYBR Green Supermix (Bio-Rad, #1725124). The relative
500 expression of each target gene was normalized to the mouse *β-actin* gene. The target
501 genes and corresponding primer sequences are shown in the Key Resource Table.
502
503 **Murine neutrophil elastase, cytokine, chemokine, and MMP profile**
504 Blood samples from each group of mice was collected by cardiac puncture
505 between 21 to 24 dpi and sera were collected. The murine neutrophil elastase level was
506 measured using the Mouse Neutrophil Elastase/ELA2 DuoSet ELISA (RnD Systems,
507 #DY4517-05). Serum was sent for cytokine analysis by the Mouse Cytokine/Chemokine
508 32-Plex Discovery Assay Array (MD32), and the Mouse MMP 5-Plex Discovery Assay
509 Array (MDMMP-S, P) performed by Eve Technologies. The cytokines and chemokines
510 represented by MD32 are Eotaxin, G-CSF, GM-CSF, IFN-γ, IL-1α, IL-1β, IL-2, IL-3, IL-4,
511 IL-5,IL-6, IL-7, IL-9, IL-10, IL-12 (p40), IL-12 (p70), IL-13, IL-15, IL-17A, IP-10, KC, LIF,
512 LIX, MCP-1, M-CSF, MIG, MIP-1α, MIP-1β, MIP-2, RANTES, TNFα, and VEGF. The

513 MMPs represented by MDMMP-S, P are MMP-2, MMP-3, MMP-8, proMMP-9, and
514 MMP-12.
515
516 **Purification of recombinant murine SLPI**
517 The murine *SLPI* cDNA ORF clone was purchased from GenScript (OMu22721).
518 The coding sequence was subsequently cloned into pET22b(+) expression vector
519 (Novagen) in frame with the pelB signal peptide using Gibson Assembly[74]. *E. coli* strain
520 Rosetta-gami 2 (DE3) (Novagen, #71351) was transformed with the SLPI-pET22b+ and
521 grown at 37°C with ampicillin (100 µg/ml), tetracycline (12.5 µg/ml), streptomycin (50
522 µg/ml) and chloramphenicol (34 µg/ml). Cells were induced with 1 mM IPTG (18°C,
523 overnight), harvested, and lysed with BugBuster Protein Extraction Reagent (Novagen,
524 #70921-3). Recombinant mSLPI was purified with a Ni-NTA resin column as described
525 by the manufacturer (Qiagen). To evaluate the activity of the purified rmSLPI, the trypsin
526 inhibitory activity was assayed with the fluorescent substrate Mca-RPKPVE-Nval-
527 WRK(Dnp)-NH2 Fluorogenic MMP Substrate (R&D Systems, #ES002) and the
528 absorbance was monitored at 405 nm using a fluorescent plate reader (Tecan).
529
530 **Flow cytometry to validate *B. burgdorferi*-SLPI binding**
531 Actively growing low passage *B. burgdorferi* was cultured to a density of 10^6–10^7
532 cells/ml and harvested at 10,000 g for 10 min. Cells were rinsed twice with PBS and
533 blocked in 1%BSA for 1 h at 4°C. The cells were pelleted, rinsed, resuspended, and
534 incubated with 10 nM and 1 µM human SLPI (R&D Systems, #1274-PI-100) and murine
535 SLPI (produced in lab as described above) at 4°C for 2 h. The binding was detected

536 with goat anti human or murine SLPI (R&D Systems, #AF1274 and AF1735) and Alexa
537 Fluor 488 or Alexa Fluor 647 donkey anti goat IgG (H+L) (Invitrogen, #A32814, A-
538 21447). The samples were fixed with 2% PFA before running through BD LSRII Green
539 (BD bioscience). The data was then analyzed by FlowJo. Permeabilization was not
540 performed during this protocol. Thus, the binding detected was on the bacterial outer
541 surface.
542
543 **ELISA to validate *B. burgdorferi*-SLPI binding**
544 *B. burgdorferi* was cultured to a density of 10^6–10^7 cells/ml and harvested at
545 10,000 g for 10 min. To make the *B. burgdorferi* lysate, cells were rinsed twice with PBS,
546 pelleted, and lysed using BugBuster Protein Extraction Reagent (Novagen, #70921-3).
547 Protein concentration in the lysate was measured by absorbance at 280 nm using the
548 nanodrop (Fisher Scientific). For the protease assay, the *B. burgdorferi* lysate was
549 incubated in the presence or absence of proteinase K (0.2 mg/ml, Thermo Scientific,
550 #EO0491) for 10 min. In an immuno 96-well plate (MaxiSorp), wells were coated with
551 200 ng of *B. burgdorferi* lysate. Samples were blocked with 1% BSA followed by
552 incubation with human SLPI at varying concentrations (1–1000 ng) for 1 h at room
553 temperature. The binding was probed with goat anti human SLPI (R&D Systems,
554 #AF1274) and rabbit anti goat IgG (whole molecule)-Peroxidases antibody (Sigma-
555 Aldrich, #A8919-2ML). KPL Sureblue TMB Microwell Peroxidase substrate, 1-
556 component (Seracare, #5120-0077) was used. The reaction was stopped with KPL TMB
557 stop solution (Seracare, #5150-0021), and absorbance was read at 450 nm.
558

559 **Immunofluorescence assay**

560 Actively growing low passage *B. burgdorferi* was cultured to a density of 10^6–10^7
561 cells/ml, rinsed twice with PBS and blocked with 1% BSA for 1 h at 4°C. *B. burgdorferi*
562 was incubated with human or murine SLPI at 4°C for 2 h. The spirochetes were probed
563 with goat anti human or murine SLPI (R&D Systems, #AF1274 and AF1735) and Alexa
564 Fluor 488 donkey anti goat IgG (H+L) (Invitrogen, #A32814). *B. burgdorferi* were then
565 stained with Hoechst 33342 (Invitrogen, #H1399). The samples were fixed with in 2%
566 PFA before imaged with Leica SP8. Permeabilization was not performed during this
567 protocol. Thus, the binding detected was on the bacterial outer surface.

568

569 **The BacTiter Glo microbial cell viability assay to quantify *B. burgdorferi* viability**

570 The BacTiter Glo microbial cell viability assay quantifies the ATP present in the
571 microbial culture by measuring luminescence. The amount of ATP is proportional to the
572 number of viable cells in culture[40,45,75]. To test the borreliacidal activity of human SLPI,
573 $1x10^5$ spirochetes were treated with 0–10 μM hSLPI (R&D Systems, #1274-PI-100) at
574 33°C for 48 h. The luminescence was measured using a fluorescence plate reader
575 (Tecan). The percent viability was normalized to the control spirochetes culture without
576 hSLPI treatment. To test the effect of hSLPI on the antibody-mediated *B. burgdorferi*
577 killing, $1x10^5$ spirochetes were pretreated with 0–5 μM hSLPI (R&D Systems, #1274-PI-
578 100) at 33°C for 2 h. 20% mouse *B. burgdorferi* antisera were then added and
579 incubated for 2 and 4 h. The mouse antisera were collected from *B. burgdorferi* infected
580 mice between 21 to 24 dpi. The luminescence was measured as described above. The
581 percent viability was normalized to the control spirochetes culture without any treatment.

582

583 **Statistical analysis**

584 The analysis of all data was performed using the non-parametric Mann-Whitney,
585 or ANOVA using Prism 10 software (GraphPad Software, Inc., San Diego, CA). A *p*-
586 value of <0.05 was considered statistically significant.

587

588 **ACKNOWLEGMENTS**

589

590 We are grateful to Dr. Narasimhan for her input and suggestions during
591 experiment design, and to Dr. Ming-Jie Wu for his assistance in conducting
592 experiments. We are grateful to Ms. Ming Li for her effort in preparing human sera
593 samples. This work was supported by NIH grants AI165499 and AI138949, the Steven
594 and Alexandra Cohen Foundation, and the Howard Hughes Medical Institute Emerging
595 Pathogens Initiative.

596

597 **AUTHOR CONTRIBUTIONS**

598

599 QY and EF designed, performed, and analyzed experiments and draft the
600 manuscript. XT designed and performed experiments. TH performed the BASEHIT
601 library screen. RH scored the severity of murine ankle inflammation. AB and LB
602 provided sera from Lyme disease patients and edited the manuscript. AN provided the
603 *SLPI*-/- mice. AR developed the BASEHIT screen. EF scored the visual swelling level of
604 murine tibiotarsal joints and supervised the research.

605

606 **Figure Legends**

607

608 **Figure 1. *B. burgdorferi* burden in C57BL/6 WT and *SLPI*-/- mice.** WT and *SLPI*-/-
609 mice were infected with 10^5 spirochetes by subcutaneous injection. (A-C) Spirochete
610 burden in skin was assessed by ear punch biopsies at 7d (A) 14 d (B), and between 21
611 to 24 d (C) post infection. (D and E) Spirochete burden in tibiotarsal joint and heart
612 tissues was assessed between 21 to 24 d (D, heart, E, joint) post infection. At least n =
613 6 mice were infected in each group. The spirochete burden was measured by qPCR
614 detecting *flaB* and normalized to mouse *β-actin*. Each data point represents an
615 individual animal. Representative data were shown from three separate experiments.
616 The error bars represent mean ± SEM and *p*-values are calculated using the non-
617 parametric Mann-Whitney test.

618

619 **Figure 2. Assessment of ankle inflammation in WT and *SLPI*-/- mice infected with**
620 ***B. burgdorferi* between 21 to 24 dpi.** (A) Representative images are shown of the
621 tibiotarsal joints of WT and *SLPI*-/- mice with/without *B. burgdorferi* infection between 21
622 to 24 dpi. The swelling is indicated by the red arrow. (B) Swelling of the tibiotarsal joints
623 of individual mice was scored visually by an observer blinded to the experimental
624 groups (scale of 0 (negative) to 3 (severe)). (C) The tibiotarsal joint of each mouse was
625 dissected, fixed, sectioned, and stained with H&E. Representative images from *B.*
626 *burgdorferi*-infected C57BL/6 WT and *SLPI*-/- mice are shown. Lower magnification (left
627 panels, Scale bar: 100 μm) and higher magnification (right panels, Scale bar: 50 μm) of

628 selected areas (black rectangle) are shown. (D) The severity of periarticular
629 inflammation was scored blindly by the pathologist on a scale of 0 (negative) to 3
630 (severe). black, PBS-sham infection; red, *B. burgdorferi* infection. Results from two
631 independent experiments were pooled and shown here. The error bars represent mean
632 ± SEM and *p*-values are calculated using the non-parametric Mann-Whitney test.
633
634 **Figure 3. Immune profile analysis of infected WT and *SLPI*-/- mice.** (A, B) Infiltrating
635 cell population analysis of tibiotarsal joint tissues of infected WT and *SLPI*-/- mice. (A)
636 The neutrophil population was gated on the CD11bLY6G double positive cells among
637 the CD45 positive cells. (B) The macrophage population was gated on the CD64
638 positive cells among the CX3CR1 positive myeloid cells. Results from two independent
639 experiments were pooled and shown here. (C-E) Expression levels of C-X-C motif
640 chemokine receptor 2 (*CXCR2*, C), monocyte chemoattractant protein 1 (*MCP-1*, D),
641 and C-C motif chemokine receptor 2 (*CCR2*, E) were assessed in the tibiotarsal tissue
642 using RT-qPCR. (F) The serum cytokine profile was assessed using mouse
643 cytokine/chemokine 32-plex array. An increase in IL-6 was observed in the infected
644 *SLPI*-/- mice. (G, H) The serum level of neutrophil elastase (NE) was measured using
645 an ELISA kit. (I) Serum levels of MMPs were assessed using a mouse MMP 5-Plex
646 Discovery Assay. An increase in MMP-8 was observed in the infected *SLPI*-/- mice.
647 Serum was obtained by cardiac puncture of WT and *SLPI*-/- C57BL/6 mice with/without
648 infection between 21 to 24 dpi (F, G, and I) and of infected C3H/HeN mice at 21 dpi (H).
649 black, PBS-sham infection; red, *B. burgdorferi* infection. Each data point represents an

650 individual animal. The error bar represents mean ± SEM and *p*-values are calculated
651 using the non-parametric Mann-Whitney test.
652
653 **Figure 4. Serum SLPI levels in Lyme disease subjects versus healthy controls.**
654 The serum level of SLPI was measured by ELISA. Sera samples were from 5 adult
655 healthy controls (HC). 18 samples were from people with Lyme disease (LD) including 5
656 samples from 3 subjects presenting with Lyme arthritis (red) and 13 samples from 4
657 subjects with erythema migrans (black). The error bar represents mean ± SEM and *p*-
658 values are calculated using the non-parametric Mann-Whitney test.
659
660 **Figure 5. *B. burgdorferi* interaction with human and murine SLPI.** (A) Sandwich
661 ELISA results show the interaction of *B. burgdorferi* whole cell lysates with human SLPI.
662 ELISA plates were coated with *B. burgdorferi* whole cell lysates and probed with
663 increasing amount of human SLPI (blue) or human Fc proteins (black) as the negative
664 control. The values plotted represent the mean ± SEM of duplicates from two
665 experiments. *P*-value is displayed in the graph and determined using the non-
666 parametric Mann-Whitney test. (B and C) Flow cytometry histograms show binding of
667 human (B) and murine (C) SLPI to *B. burgdorferi* cultured at 33°C (solid line) and 37°C
668 (dash line). *B. burgdorferi* was cultured to a density of 10^6/ml. The same volume of
669 cultures was incubated at 33°C or 37°C for 24 hrs before adding 10 nM (green) or 1 μM
670 (red) human or murine SLPI. The binding was detected with goat anti human or murine
671 SLPI and donkey anti goat AF647 or AF488. *B. burgdorferi* alone (grey) and antibody
672 control (without SLPI, blue) were used as negative controls. (D) Immuno-fluorescent

673 microscopy was used to directly observe the binding of *B. burgdorferi* with human and
674 murine SLPI. Merged and single-color images are shown. Representative histograms
675 and fluorescent images were shown from three independent experiments. Scale bar: 10
676 μm.
677
678 **Supplemental Figure 1. The macrophages population analyzed using Ly6G-**
679 **negative gating strategy.** The macrophage population was first gated on the Ly6G-
680 negative population, then gated on the CD64 positive cells among the CX3CR1 positive
681 myeloid cells. Results from two independent experiments were pooled and shown here.
682
683 **Supplemental Figure 2. The binding of human SLPI to non-infectious *B.***
684 ***burgdorferi B31A* and proteinase K-treated *B. burgdorferi B31A3*.** (A) Flow
685 cytometry histogram shows the lack of binding of human SLPI (1 μM, red) to non-
686 infectious *B. burgdorferi B31A. B. burgdorferi* alone (grey) and antibody control (without
687 SLPI, blue) were used as negative controls. A representative histogram from two
688 independent experiments was shown. (B) ELISA result shows the interaction between
689 human SLPI and *B. burgdorferi B31A3* whole cell lysates in the presence (blue) or
690 absence (black) of proteinase K. ELISA plates were coated with *B. burgdorferi B31A3*
691 whole cell lysates and probed with increasing amount of human SLPI. The values
692 plotted represent the mean ± SEM of triplicates from one experiment.
693
694 **Supplemental Figure 3. The effect of human SLPI binding on *B. burgdorferi***
695 **viability and antibody-mediated killing.** (A) Human SLPI (hSLPI, 0-10 μM) was

696 incubated with 10^5 *B. burgdorferi* at 33°C for 48 hours. The viability was assessed by
697 BacTiter Glo microbial cell viability assay. The percent viability was normalized to the
698 control spirochetes culture without hSLPI treatment. Results from one independent
699 experiment performed in triplicate samples are shown here. (B) Human SLPI (hSLPI, 0-
700 5 μM) was incubated with 10^5 *B. burgdorferi* at 33°C for 2 hours. 20% mouse *B.*
701 *burgdorferi* antisera were then added for 2 and 4 h. The viability was measured as
702 described above. The percent viability was normalized to the control spirochetes culture
703 without any treatment. Results from two independent experiments performed in
704 duplicate samples are shown here.
705
706 **Supplemental Figure 4. Serum and gene expression levels of TNF-α.** (A) The serum
707 level of TNF-α was assessed using a mouse cytokine/chemokine 32-plex array. (B) The
708 gene expression level of TNF-α was assessed in the tibiotarsal tissue using RT-qPCR.
709 Serum was obtained by cardiac puncture and the tibiotarsal tissue was collected from
710 WT and *SLPI*-/- C57BL/6 mice with/without *B. burgdorferi* infection between 21 to 24
711 dpi. black, PBS-sham infection; red, *B. burgdorferi* infection. Each data point represents
712 an individual animal. The error bar represents mean ± SEM and *p*-values, and were
713 calculated using the non-parametric Mann-Whitney test.
714
715 **Supplemental Table 1. Subject Characterization**
716
717 **Supplemental Table 2. The primers used in this study.**
718

Key resources table

Reagent type (species) or resource	Designation	Source or reference	IDENTIFIER
Antibodies	TruStain FcXTM anti-mouse CD16/32	BioLegend	Cat#101320
Antibodies	PerCP anti-mouse CD45	BioLegend	Cat#103130
Antibodies	BV711 anti-mouse Ly6G	BioLegend	Cat#127643
Antibodies	PE anti-mouse CD11b	BioLegend	Cat#101208
Antibodies	APC/CY7 anti-mouse CX3CR21	BioLegend	Cat#149047
Antibodies	FITC anti-mouse Ly6C	BioLegend	Cat#128005
Antibodies	APC anti-mouse CD64	BioLegend	Cat#139305
Antibodies	goat anti human SLPI	R&D Systems	Cat#AF1274
Antibodies	goat anti murine SLPI	R&D Systems	Cat#AF1735
Antibodies	Alexa Fluor 488 donkey anti goat IgG (H+L)	Invitrogen	Cat#A32814
Antibodies	Alexa Fluor 647 donkey anti goat IgG (H+L)	Invitrogen	Cat#A-21447
Bacterial strains	*Borrelia. burgdorferi* B31-A3	Dr. Utpal Pal's laboratory	N/A
Bacterial strains	*Borrelia. burgdorferi* B31-A	This manuscript	N/A
Bacterial strains	*E. coli* Rosetta-gami 2 (DE3) competent cell	Novagen	Cat#71351
Biological samples	Mouse tibiotarsal tissue	This manuscript	N/A
Recombinant proteins	human SLPI	R&D Systems	Cat#1274-PI-100
Chemical	iQ SYBR Green Supermix	Bio-Rad	Cat#1725124
Chemical	Barbour-Stoenner-Kelly H (BSK-H) complete medium	Sigma-Aldrich	Cat#B8291
Chemical	Bouin's solution	Sigma-Aldrich	Cat#HT10132
Chemical	Hyaluronidase	Sigma-Aldrich	Cat#H3506
Chemical	Collagenase	Sigma-Aldrich	Cat#C2139
Chemical	ACK Lysing buffer	Gibco	Cat#A1049201
Chemical	Trizol	Invitrogen,	Cat#15596-018
peptide	Mca-RPKPVE-Nval-WRK(Dnp)-NH2 Fluorogenic MMP Substrate	R&D Systems	Cat#ES002
Chemical	BugBuster Protein Extraction Reagent	Novagen	Cat#70921-3
Chemical	Proteinase K	Thermo Scientific	Cat#EO0491
Chemical	Ni-NTA agarose	QIAGEN	Cat#30230
Chemical	KPL Sureblue TMB Microwell Peroxidase substrate, 1-component	Seracare	Cat#5120-0077

Chemical	KPL TMB stop solution	Seracare	Cat#5150-0021
Chemical	Hoechst 33342	Invitrogen	Cat#H1399
Chemical	RPMI 1640	Gibco	Cat#11875-093
Critical commercial assays	LIVE/DEADTM fixable violet stain kit	Invitrogen	Cat#L34955
Critical commercial assays	iScript cDNA Synthesis Kit	Bio-Rad	Cat#1708891
Critical commercial assays	DNeasy Blood & Tissue Kit	Qiagen	
Critical commercial assays	Gibson Assembly Kit	NEB	
Critical commercial assays	Mouse Neutrophil Elastase/ELA2 DuoSet ELISA	RnD Systems	Cat#DY4517-05
Critical commercial assays	Human SLPI DuoSet ELISA	RnD Systems	Cat#DY1274-05
Critical commercial assays	BacTiter-Glo Microbial Cell Viability Assay kit	Promega	Cat#G8230
Critical commercial assays	Mouse MMP 5-Plex Discovery Assay Array (MDMMP-S, P)	Eve Technologies	N/A
Critical commercial assays	Mouse Cytokine/Chemokine 32-Plex Discovery Assay Array (MD32)	Eve Technologies	N/A
Experimental models: Organisms/strains	*SLPI-/-* mice	Dr. Akira Nakamura's laboratory[68, 69]	https://doi.org/10.3389/fimmu.2017.01538 https://doi.org/10.1084/jem.20021824
Experimental models: Organisms/strains	C3H/HeN mice	Charles River Laboratories	N/A
Experimental models: Organisms/strains	C57BL/6 mice	Jackson Laboratory	Stock #: 000664; RRID: IMSR_JAX:000664
Recombinant DNA	Plasmid: Murine *SLPI* cDNA ORF clone	GenScript	OMu22721
Recombinant DNA	Plasmid: pET-22b (+)	Novagen	Cat#69744-3
Software and algorithms	Prism	GraphPad	RRID:SCR_002798
Software and algorithms	FlowJo	BD Biosciences	https://www.flowjo.com/

723

724 **References**

725 1. Kugeler, K.J., Schwartz, A.M., Delorey, M.J., Mead, P.S., and Hinckley, A.F. (2021).
726 Estimating the frequency of Lyme disease diagnoses, United States, 2010–2018.
727 Emerging Infectious Diseases *27*, 616.
728 2. Mead, P. (2022). Epidemiology of Lyme Disease. Infect Dis Clin North Am *36*, 495-521.
729 10.1016/j.idc.2022.03.004.
730 3. Arvikar, S.L., and Steere, A.C. (2022). Lyme arthritis. Infectious Disease Clinics *36*, 563-
731 577.
732 4. Schwartz, A.M., Hinckley, A.F., Mead, P.S., Hook, S.A., and Kugeler, K.J. (2017).
733 Surveillance for Lyme Disease - United States, 2008-2015. MMWR Surveill Summ *66*, 1-
734 12. 10.15585/mmwr.ss6622a1.
735 5. Steere, A.C., Schoen, R.T., and Taylor, E. (1987). The clinical evolution of Lyme arthritis.
736 Ann Intern Med *107*, 725-731. 10.7326/0003-4819-107-5-725.
737 6. Miller, J.B., and Aucott, J.N. (2021). Stages of Lyme Arthritis. J Clin Rheumatol *27*, e540-
738 e546. 10.1097/RHU.0000000000001513.
739 7. Lochhead, R.B., Strle, K., Arvikar, S.L., Weis, J.J., and Steere, A.C. (2021). Lyme arthritis:
740 linking infection, inflammation and autoimmunity. Nature Reviews Rheumatology *17*,
741 449-461.
742 8. Shin, J.J., Glickstein, L.J., and Steere, A.C. (2007). High levels of inflammatory chemokines
743 and cytokines in joint fluid and synovial tissue throughout the course of antibiotic-
744 refractory lyme arthritis. Arthritis Rheum *56*, 1325-1335. 10.1002/art.22441.
745 9. Lochhead, R.B., Ordoñez, D., Arvikar, S.L., Aversa, J.M., Oh, L.S., Heyworth, B., Sadreyev,
746 R., Steere, A.C., and Strle, K. (2019). Interferon-gamma production in Lyme arthritis
747 synovial tissue promotes differentiation of fibroblast-like synoviocytes into immune
748 effector cells. Cell Microbiol *21*, e12992. 10.1111/cmi.12992.
749 10. Gross, D.M., Steere, A.C., and Huber, B.T. (1998). T helper 1 response is dominant and
750 localized to the synovial fluid in patients with Lyme arthritis. J Immunol *160*, 1022-1028.
751 11. Lochhead, R.B., Arvikar, S.L., Aversa, J.M., Sadreyev, R.I., Strle, K., and Steere, A.C. (2019).
752 Robust interferon signature and suppressed tissue repair gene expression in synovial
753 tissue from patients with postinfectious, Borrelia burgdorferi-induced Lyme arthritis. Cell
754 Microbiol *21*, e12954. 10.1111/cmi.12954.
755 12. Barthold, S.W., Beck, D.S., Hansen, G.M., Terwilliger, G.A., and Moody, K.D. (1990). Lyme
756 borreliosis in selected strains and ages of laboratory mice. J Infect Dis *162*, 133-138.
757 10.1093/infdis/162.1.133.
758 13. Barthold, S.W. (1996). Lyme borreliosis in the laboratory mouse.
759 14. Ma, Y., Seiler, K.P., Eichwald, E.J., Weis, J.H., Teuscher, C., and Weis, J.J. (1998). Distinct
760 characteristics of resistance to Borrelia burgdorferi-induced arthritis in C57BL/6N mice.
761 Infect Immun *66*, 161-168. 10.1128/IAI.66.1.161-168.1998.
762 15. Brown, C.R., and Reiner, S.L. (1999). Genetic control of experimental Lyme arthritis in the
763 absence of specific immunity. Infection and immunity *67*, 1967-1973.

764 16. Ritzman, A.M., Hughes-Hanks, J.M., Blaho, V.A., Wax, L.E., Mitchell, W.J., and Brown, C.R.
765 (2010). The chemokine receptor CXCR2 ligand KC (CXCL1) mediates neutrophil
766 recruitment and is critical for development of experimental Lyme arthritis and carditis.
767 Infect Immun *78*, 4593-4600. 10.1128/IAI.00798-10.
768 17. Miller, J.C., Ma, Y., Bian, J., Sheehan, K.C., Zachary, J.F., Weis, J.H., Schreiber, R.D., and
769 Weis, J.J. (2008). A critical role for type I IFN in arthritis development following Borrelia
770 burgdorferi infection of mice. J Immunol *181*, 8492-8503.
771 10.4049/jimmunol.181.12.8492.
772 18. Brown, C.R., Blaho, V.A., and Loiacono, C.M. (2003). Susceptibility to experimental Lyme
773 arthritis correlates with KC and monocyte chemoattractant protein-1 production in joints
774 and requires neutrophil recruitment via CXCR2. J Immunol *171*, 893-901.
775 10.4049/jimmunol.171.2.893.
776 19. Anguita, J., Barthold, S.W., Persinski, R., Hedrick, M.N., Huy, C.A., Davis, R.J., Flavell, R.A.,
777 and Fikrig, E. (2002). Murine Lyme arthritis development mediated by p38 mitogen-
778 activated protein kinase activity. J Immunol *168*, 6352-6357.
779 10.4049/jimmunol.168.12.6352.
780 20. Doumas, S., Kolokotronis, A., and Stefanopoulos, P. (2005). Anti-inflammatory and
781 antimicrobial roles of secretory leukocyte protease inhibitor. Infect Immun *73*, 1271-
782 1274. 10.1128/IAI.73.3.1271-1274.2005.
783 21. Thompson, R.C., and Ohlsson, K. (1986). Isolation, properties, and complete amino acid
784 sequence of human secretory leukocyte protease inhibitor, a potent inhibitor of
785 leukocyte elastase. Proc Natl Acad Sci U S A *83*, 6692-6696. 10.1073/pnas.83.18.6692.
786 22. Moreau, T., Baranger, K., Dadé, S., Dallet-Choisy, S., Guyot, N., and Zani, M.L. (2008).
787 Multifaceted roles of human elafin and secretory leukocyte proteinase inhibitor (SLPI),
788 two serine protease inhibitors of the chelonianin family. Biochimie *90*, 284-295.
789 10.1016/j.biochi.2007.09.007.
790 23. Maruyama, M., Hay, J.G., Yoshimura, K., Chu, C.S., and Crystal, R.G. (1994). Modulation
791 of secretory leukoprotease inhibitor gene expression in human bronchial epithelial cells
792 by phorbol ester. J Clin Invest *94*, 368-375. 10.1172/JCI117331.
793 24. Sallenave, J.M., Shulmann, J., Crossley, J., Jordana, M., and Gauldie, J. (1994). Regulation
794 of secretory leukocyte proteinase inhibitor (SLPI) and elastase-specific inhibitor
795 (ESI/elafin) in human airway epithelial cells by cytokines and neutrophilic enzymes. Am J
796 Respir Cell Mol Biol *11*, 733-741. 10.1165/ajrcmb.11.6.7946401.
797 25. Ashcroft, G.S., Lei, K., Jin, W., Longenecker, G., Kulkarni, A.B., Greenwell-Wild, T., Hale-
798 Donze, H., McGrady, G., Song, X.Y., and Wahl, S.M. (2000). Secretory leukocyte protease
799 inhibitor mediates non-redundant functions necessary for normal wound healing. Nat
800 Med *6*, 1147-1153. 10.1038/80489.
801 26. Zhu, J., Nathan, C., Jin, W., Sim, D., Ashcroft, G.S., Wahl, S.M., Lacomis, L., Erdjument-
802 Bromage, H., Tempst, P., Wright, C.D., and Ding, A. (2002). Conversion of proepithelin to
803 epithelins: roles of SLPI and elastase in host defense and wound repair. Cell *111*, 867-
804 878. 10.1016/s0092-8674(02)01141-8.
805 27. Taggart, C.C., Cryan, S.A., Weldon, S., Gibbons, A., Greene, C.M., Kelly, E., Low, T.B.,
806 O'neill, S.J., and McElvaney, N.G. (2005). Secretory leucoprotease inhibitor binds to NF-

807 kappaB binding sites in monocytes and inhibits p65 binding. J Exp Med *202*, 1659-1668.
808 10.1084/jem.20050768.
809 28. Taggart, C.C., Greene, C.M., McElvaney, N.G., and O'Neill, S. (2002). Secretory
810 leucoprotease inhibitor prevents lipopolysaccharide-induced IkappaBalpha degradation
811 without affecting phosphorylation or ubiquitination. J Biol Chem *277*, 33648-33653.
812 10.1074/jbc.M203710200.
813 29. Jin, F.Y., Nathan, C., Radzioch, D., and Ding, A. (1997). Secretory leukocyte protease
814 inhibitor: a macrophage product induced by and antagonistic to bacterial
815 lipopolysaccharide. Cell *88*, 417-426. 10.1016/s0092-8674(00)81880-2.
816 30. Huet, G., Flipo, R.M., Richet, C., Thiebaut, C., Demeyer, D., Balduyck, M., Duquesnoy, B.,
817 and Degand, P. (1992). Measurement of elastase and cysteine proteinases in synovial
818 fluid of patients with rheumatoid arthritis, sero-negative spondylarthropathies, and
819 osteoarthritis. Clin Chem *38*, 1694-1697.
820 31. Wilkinson, D.J., Arques, M.D.C., Huesa, C., and Rowan, A.D. (2019). Serine proteinases in
821 the turnover of the cartilage extracellular matrix in the joint: implications for
822 therapeutics. Br J Pharmacol *176*, 38-51. 10.1111/bph.14173.
823 32. McDonnell, J., Lobner, J.M., Knight, W.B., Lark, M.W., Green, B., Poe, M., and Moore, V.L.
824 (1993). Comparison of the proteoglycanolytic activities of human leukocyte elastase and
825 human cathepsin G in vitro and in vivo. Connect Tissue Res *30*, 1-9.
826 10.3109/03008209309032926.
827 33. Lee, S.-Y., Nho, T.-H., Choi, B.-D., Jeong, S.-J., Lim, D.-S., and Jeong, M.-J. (2016).
828 Secretory leukocyte protease inhibitor reduces inflammation and alveolar bone
829 resorption in LPS-induced periodontitis in rats and in MC3T3-E1 preosteoblasts. Animal
830 Cells and Systems *20*, 344-352. 10.1080/19768354.2016.1250817.
831 34. Song, X., Zeng, L., Jin, W., Thompson, J., Mizel, D.E., Lei, K., Billinghurst, R.C., Poole, A.R.,
832 and Wahl, S.M. (1999). Secretory leukocyte protease inhibitor suppresses the
833 inflammation and joint damage of bacterial cell wall-induced arthritis. J Exp Med *190*,
834 535-542. 10.1084/jem.190.4.535.
835 35. Akitsu, A., and Iwakura, Y. (2016). Isolation of Joint-infiltrating Cells. Bio-protocol *6*,
836 e1911-e1911.
837 36. Feng, G., Zhu, C., Lin, C.Y., Bredemeyer, A., Förster, I., Kreisel, D., and Lavine, K.J. (2023).
838 CCL17 Protects Against Viral Myocarditis by Suppressing the Recruitment of Regulatory T
839 Cells. J Am Heart Assoc *12*, e028442. 10.1161/JAHA.122.028442.
840 37. Srirangan, S., and Choy, E.H. (2010). The role of interleukin 6 in the pathophysiology of
841 rheumatoid arthritis. Ther Adv Musculoskelet Dis *2*, 247-256.
842 10.1177/1759720X10378372.
843 38. Murphy, G., and Nagase, H. (2008). Reappraising metalloproteinases in rheumatoid
844 arthritis and osteoarthritis: destruction or repair? Nat Clin Pract Rheumatol *4*, 128-135.
845 10.1038/ncprheum0727.
846 39. Hu, L.T., Eskildsen, M.A., Masgala, C., Steere, A.C., Arner, E.C., Pratta, M.A., Grodzinsky,
847 A.J., Loening, A., and Perides, G. (2001). Host metalloproteinases in Lyme arthritis.
848 Arthritis Rheum *44*, 1401-1410. 10.1002/1529-0131(200106)44:6<1401::AID-
849 ART234>3.0.CO;2-S.

850 40. Gupta, A., Arora, G., Rosen, C.E., Kloos, Z., Cao, Y., Cerny, J., Sajid, A., Hoornstra, D.,
851 Golovchenko, M., Rudenko, N., et al. (2020). A human secretome library screen reveals a
852 role for Peptidoglycan Recognition Protein 1 in Lyme borreliosis. PLoS Pathog *16*,
853 e1009030. 10.1371/journal.ppat.1009030.
854 41. Shi, Y., Xu, Q., McShan, K., and Liang, F.T. (2008). Both decorin-binding proteins A and B
855 are critical for the overall virulence of Borrelia burgdorferi. Infect Immun *76*, 1239-1246.
856 10.1128/IAI.00897-07.
857 42. Li, X., Liu, X., Beck, D.S., Kantor, F.S., and Fikrig, E. (2006). Borrelia burgdorferi lacking
858 BBK32, a fibronectin-binding protein, retains full pathogenicity. Infect Immun *74*, 3305-
859 3313. 10.1128/IAI.02035-05.
860 43. Koenigs, A., Hammerschmidt, C., Jutras, B.L., Pogoryelov, D., Barthel, D., Skerka, C.,
861 Kugelstadt, D., Wallich, R., Stevenson, B., Zipfel, P.F., and Kraiczy, P. (2013). BBA70 of
862 Borrelia burgdorferi is a novel plasminogen-binding protein. J Biol Chem *288*, 25229-
863 25243. 10.1074/jbc.M112.413872.
864 44. Sonnert, N.D., Rosen, C.E., Ghazi, A.R., Franzosa, E.A., Duncan-Lowey, B., González-
865 Hernández, J.A., Huck, J.D., Yang, Y., Dai, Y., Rice, T.A., et al. (2024). A host-microbiota
866 interactome reveals extensive transkingdom connectivity. Nature *628*, 171-179.
867 10.1038/s41586-024-07162-0.
868 45. Arora, G., Lynn, G.E., Tang, X., Rosen, C.E., Hoornstra, D., Sajid, A., Hovius, J.W., Palm,
869 N.W., Ring, A.M., and Fikrig, E. (2022). CD55 Facilitates Immune Evasion by Borrelia
870 crocidurae, an Agent of Relapsing Fever. mBio *13*, e0116122. 10.1128/mbio.01161-22.
871 46. Hart, T.M., Sonnert, N.D., Tang, X., Chaurasia, R., Allen, P.E., Hunt, J.R., Read, C.B.,
872 Johnson, E.E., Arora, G., Dai, Y., et al. (2024). An atlas of human vector-borne microbe
873 interactions reveals pathogenicity mechanisms. Cell. 10.1016/j.cell.2024.05.023.
874 47. Caine, J.A., and Coburn, J. (2015). A short-term Borrelia burgdorferi infection model
875 identifies tissue tropisms and bloodstream survival conferred by adhesion proteins.
876 Infect Immun *83*, 3184-3194. 10.1128/IAI.00349-15.
877 48. Elias, A.F., Stewart, P.E., Grimm, D., Caimano, M.J., Eggers, C.H., Tilly, K., Bono, J.L., Akins,
878 D.R., Radolf, J.D., Schwan, T.G., and Rosa, P. (2002). Clonal polymorphism of Borrelia
879 burgdorferi strain B31 MI: implications for mutagenesis in an infectious strain
880 background. Infect Immun *70*, 2139-2150. 10.1128/IAI.70.4.2139-2150.2002.
881 49. Wiedow, O., Harder, J., Bartels, J., Streit, V., and Christophers, E. (1998).
882 Antileukoprotease in human skin: an antibiotic peptide constitutively produced by
883 keratinocytes. Biochem Biophys Res Commun *248*, 904-909. 10.1006/bbrc.1998.9069.
884 50. Nishimura, J., Saiga, H., Sato, S., Okuyama, M., Kayama, H., Kuwata, H., Matsumoto, S.,
885 Nishida, T., Sawa, Y., and Akira, S. (2008). Potent antimycobacterial activity of mouse
886 secretory leukocyte protease inhibitor. The Journal of Immunology *180*, 4032-4039.
887 51. Hiemstra, P.S., Maassen, R.J., Stolk, J., Heinzel-Wieland, R., Steffens, G.J., and Dijkman,
888 J.H. (1996). Antibacterial activity of antileukoprotease. Infect Immun *64*, 4520-4524.
889 10.1128/iai.64.11.4520-4524.1996.
890 52. Ramamoorthi, N., Narasimhan, S., Pal, U., Bao, F., Yang, X.F., Fish, D., Anguita, J., Norgard,
891 M.V., Kantor, F.S., Anderson, J.F., et al. (2005). The Lyme disease agent exploits a tick
892 protein to infect the mammalian host. Nature *436*, 573-577. 10.1038/nature03812.

893 53. Schuijt, T.J., Hovius, J.W., van Burgel, N.D., Ramamoorthi, N., Fikrig, E., and van Dam, A.P.
894 (2008). The tick salivary protein Salp15 inhibits the killing of serum-sensitive Borrelia
895 burgdorferi sensu lato isolates. Infect Immun *76*, 2888-2894. 10.1128/IAI.00232-08.
896 54. Crandall, H., Dunn, D.M., Ma, Y., Wooten, R.M., Zachary, J.F., Weis, J.H., Weiss, R.B., and
897 Weis, J.J. (2006). Gene expression profiling reveals unique pathways associated with
898 differential severity of lyme arthritis. J Immunol *177*, 7930-7942.
899 10.4049/jimmunol.177.11.7930.
900 55. Nugteren, S., and Samsom, J.N. (2021). Secretory Leukocyte Protease Inhibitor (SLPI) in
901 mucosal tissues: Protects against inflammation, but promotes cancer. Cytokine &
902 Growth Factor Reviews *59*, 22-35.
903 56. Lochhead, R.B., Strle, K., Kim, N.D., Kohler, M.J., Arvikar, S.L., Aversa, J.M., and Steere,
904 A.C. (2017). MicroRNA Expression Shows Inflammatory Dysregulation and Tumor-Like
905 Proliferative Responses in Joints of Patients With Postinfectious Lyme Arthritis. Arthritis
906 Rheumatol *69*, 1100-1110. 10.1002/art.40039.
907 57. Grillon, A., Scherlinger, M., Boyer, P.H., De Martino, S., Perdriger, A., Blasquez, A., Wipff,
908 J., Korganow, A.S., Bonnard, C., Cantagrel, A., et al. (2019). Characteristics and clinical
909 outcomes after treatment of a national cohort of PCR-positive Lyme arthritis. Semin
910 Arthritis Rheum *48*, 1105-1112. 10.1016/j.semarthrit.2018.09.007.
911 58. Deshmane, S.L., Kremlev, S., Amini, S., and Sawaya, B.E. (2009). Monocyte
912 chemoattractant protein-1 (MCP-1): an overview. J Interferon Cytokine Res *29*, 313-326.
913 10.1089/jir.2008.0027.
914 59. Lally, F., Smith, E., Filer, A., Stone, M.A., Shaw, J.S., Nash, G.B., Buckley, C.D., and Rainger,
915 G.E. (2005). A novel mechanism of neutrophil recruitment in a coculture model of the
916 rheumatoid synovium. Arthritis Rheum *52*, 3460-3469. 10.1002/art.21394.
917 60. Grillet, B., Pereira, R.V.S., Van Damme, J., Abu El-Asrar, A., Proost, P., and Opdenakker, G.
918 (2023). Matrix metalloproteinases in arthritis: towards precision medicine. Nat Rev
919 Rheumatol *19*, 363-377. 10.1038/s41584-023-00966-w.
920 61. Chang, Y.H., Lin, I.L., Tsay, G.J., Yang, S.C., Yang, T.P., Ho, K.T., Hsu, T.C., and Shiau, M.Y.
921 (2008). Elevated circulatory MMP-2 and MMP-9 levels and activities in patients with
922 rheumatoid arthritis and systemic lupus erythematosus. Clin Biochem *41*, 955-959.
923 10.1016/j.clinbiochem.2008.04.012.
924 62. Wen, G., Zhang, C., Chen, Q., Luong, l.A., Mustafa, A., Ye, S., and Xiao, Q. (2015). A Novel
925 Role of Matrix Metalloproteinase-8 in Macrophage Differentiation and Polarization. J Biol
926 Chem *290*, 19158-19172. 10.1074/jbc.M114.634022.
927 63. Lin, B., Kidder, J.M., Noring, R., Steere, A.C., Klempner, M.S., and Hu, L.T. (2001).
928 Differences in synovial fluid levels of matrix metalloproteinases suggest separate
929 mechanisms of pathogenesis in Lyme arthritis before and after antibiotic treatment. J
930 Infect Dis *184*, 174-180. 10.1086/322000.
931 64. Behera, A.K., Hildebrand, E., Scagliotti, J., Steere, A.C., and Hu, L.T. (2005). Induction of
932 host matrix metalloproteinases by Borrelia burgdorferi differs in human and murine
933 lyme arthritis. Infect Immun *73*, 126-134. 10.1128/IAI.73.1.126-134.2005.
934 65. Zakrzewicz, A., Richter, K., Zakrzewicz, D., Siebers, K., Damm, J., Agné, A., Hecker, A.,
935 McIntosh, J.M., Chamulitrat, W., Krasteva-Christ, G., et al. (2019). SLPI Inhibits ATP-

936 Mediated Maturation of IL-1β in Human Monocytic Leukocytes: A Novel Function of an
937 Old Player. Front Immunol *10*, 664. 10.3389/fimmu.2019.00664.
938 66. Grobmyer, S.R., Barie, P.S., Nathan, C.F., Fuortes, M., Lin, E., Lowry, S.F., Wright, C.D.,
939 Weyant, M.J., Hydo, L., Reeves, F., et al. (2000). Secretory leukocyte protease inhibitor,
940 an inhibitor of neutrophil activation, is elevated in serum in human sepsis and
941 experimental endotoxemia. Crit Care Med *28*, 1276-1282. 10.1097/00003246-
942 200005000-00003.
943 67. Tarhini, M.F.H., Bentaher, A., Greige-Gerges, H., and Elaissari, A. (2018). A potential new
944 strategy for using elastase and its inhibitor as therapeutic agents. J. Transl. Sci *5*, 1-8.
945 68. Takayama, K., Rothenberg, R.J., and Barbour, A.G. (1987). Absence of lipopolysaccharide
946 in the Lyme disease spirochete, Borrelia burgdorferi. Infect Immun *55*, 2311-2313.
947 10.1128/iai.55.9.2311-2313.1987.
948 69. Bernard, Q., Smith, A.A., Yang, X., Koci, J., Foor, S.D., Cramer, S.D., Zhuang, X., Dwyer, J.E.,
949 Lin, Y.P., Mongodin, E.F., et al. (2018). Plasticity in early immune evasion strategies of a
950 bacterial pathogen. Proc Natl Acad Sci U S A *115*, E3788-E3797.
951 10.1073/pnas.1718595115.
952 70. Matsuba, S., Yabe-Wada, T., Takeda, K., Sato, T., Suyama, M., Takai, T., Kikuchi, T., Nukiwa,
953 T., and Nakamura, A. (2017). Identification of Secretory Leukoprotease Inhibitor As an
954 Endogenous Negative Regulator in Allergic Effector Cells. Front Immunol *8*, 1538.
955 10.3389/fimmu.2017.01538.
956 71. Nakamura, A., Mori, Y., Hagiwara, K., Suzuki, T., Sakakibara, T., Kikuchi, T., Igarashi, T.,
957 Ebina, M., Abe, T., and Miyazaki, J. (2003). Increased susceptibility to LPS-induced
958 endotoxin shock in secretory leukoprotease inhibitor (SLPI)-deficient mice. The Journal
959 of experimental medicine *197*, 669-674.
960 72. Wilson, T., Kaur, N., Davis, J., and Ali, S.A. (2021). Tissue Collection and RNA Extraction
961 from the Human Osteoarthritic Knee Joint. J Vis Exp. 10.3791/62718.
962 73. Zheng, H., and McAlinden, A. (2021). RNA Isolation from Articular Cartilage Tissue.
963 Methods Mol Biol *2245*, 121-133. 10.1007/978-1-0716-1119-7_9.
964 74. Maffia, P.C., Zittermann, S.E., Scimone, M.L., Tateosian, N., Amiano, N., Guerrieri, D.,
965 Lutzky, V., Rosso, D., Romeo, H.E., Garcia, V.E., et al. (2007). Neutrophil elastase converts
966 human immature dendritic cells into transforming growth factor-beta1-secreting cells
967 and reduces allostimulatory ability. Am J Pathol *171*, 928-937.
968 10.2353/ajpath.2007.061043.
969 75. Schwendinger, M.G., O'Rourke, M., Traweger, A., Savidis-Dacho, H., Pilz, A., Portsmouth,
970 D., Livey, I., Barrett, P.N., and Crowe, B.A. (2013). Evaluation of OspA vaccination-induced
971 serological correlates of protection against Lyme borreliosis in a mouse model. PLoS One
972 *8*, e79022. 10.1371/journal.pone.0079022.
973

Figure 1

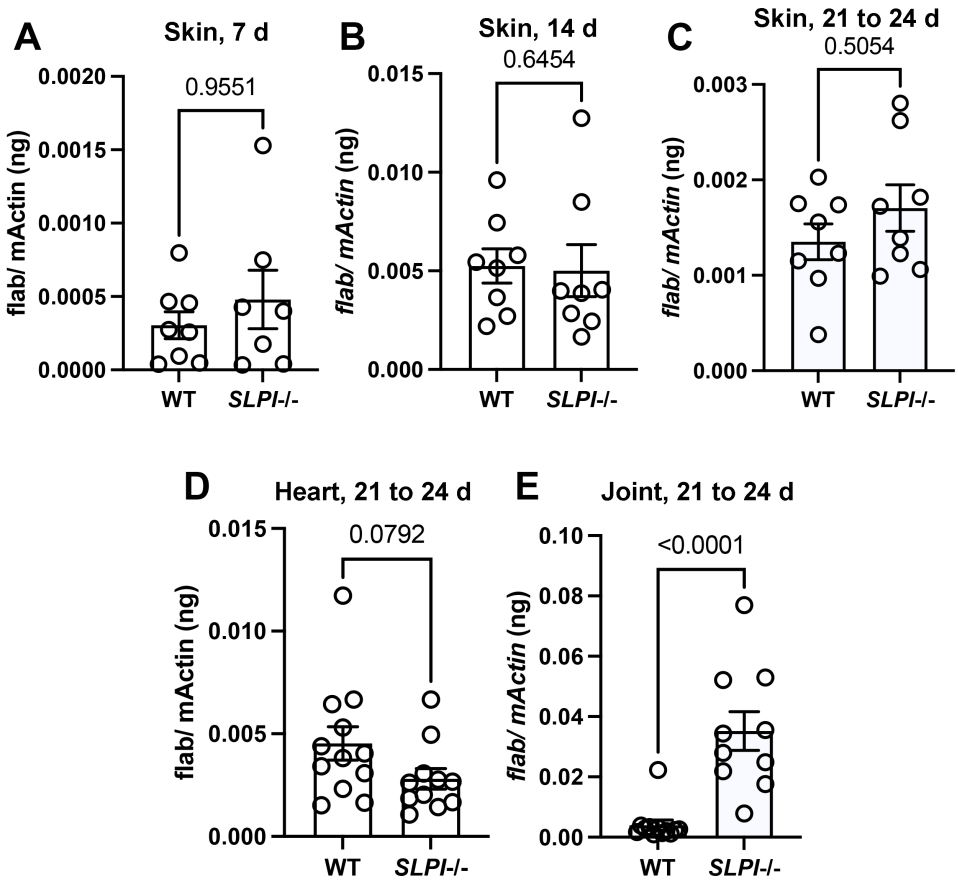
A
Skin, 7 d
0.9551
flab/ mActin (ng)
0.0020
0.0015
0.0010
0.0005
0.0000
WT
SLPI-/-
B
Skin, 14 d
0.6454
flab/ mActin (ng)
0.015
0.010
0.005
0.000
WT
SLPI-/-
C
Skin, 21 to 24 d
0.5054
flab/ mActin (ng)
0.003
0.002
0.001
0.000
WT
SLPI-/-
D
Heart, 21 to 24 d
0.0792
flab/ mActin (ng)
0.015
0.010
0.005
0.000
WT
SLPI-/-
E
Joint, 21 to 24 d
<0.0001
flab/ mActin (ng)
0.10
0.08
0.06
0.04
0.02
0.00
WT
SLPI-/-

Figure 2

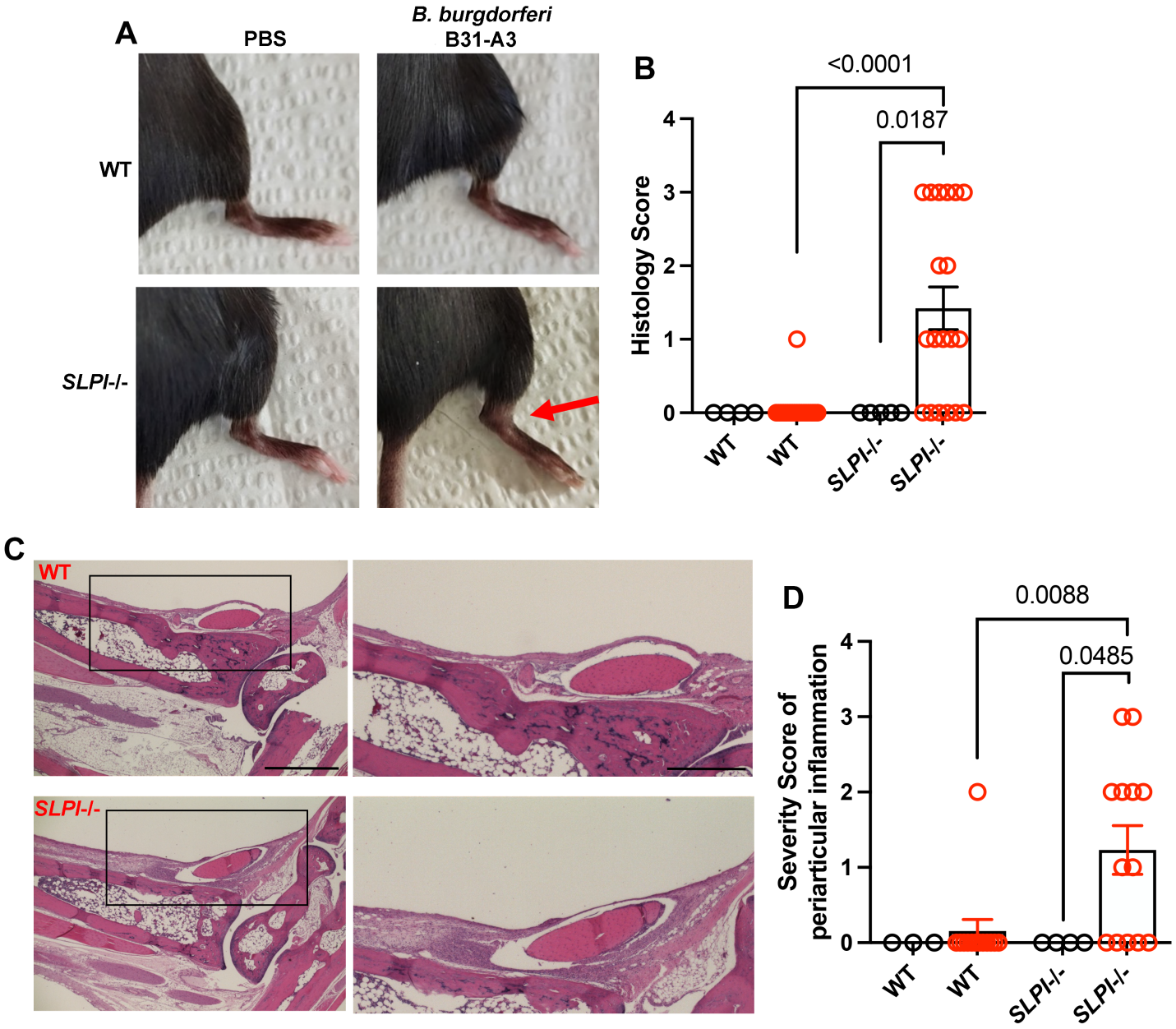
A
PBS
B. burgdorferi
B31-A3
WT
SLPI-/-
B
<0.0001
0.0187
Histology Score
4
3
2
1
0
WT
WT
SLPI-/-
SLPI-/-
C
WT
SLPI-/-
D
0.0088
0.0485
Severity Score of periarticular inflammation
4
3
2
1
0
WT
WT
SLPI-/-
SLPI-/-

Figure 3

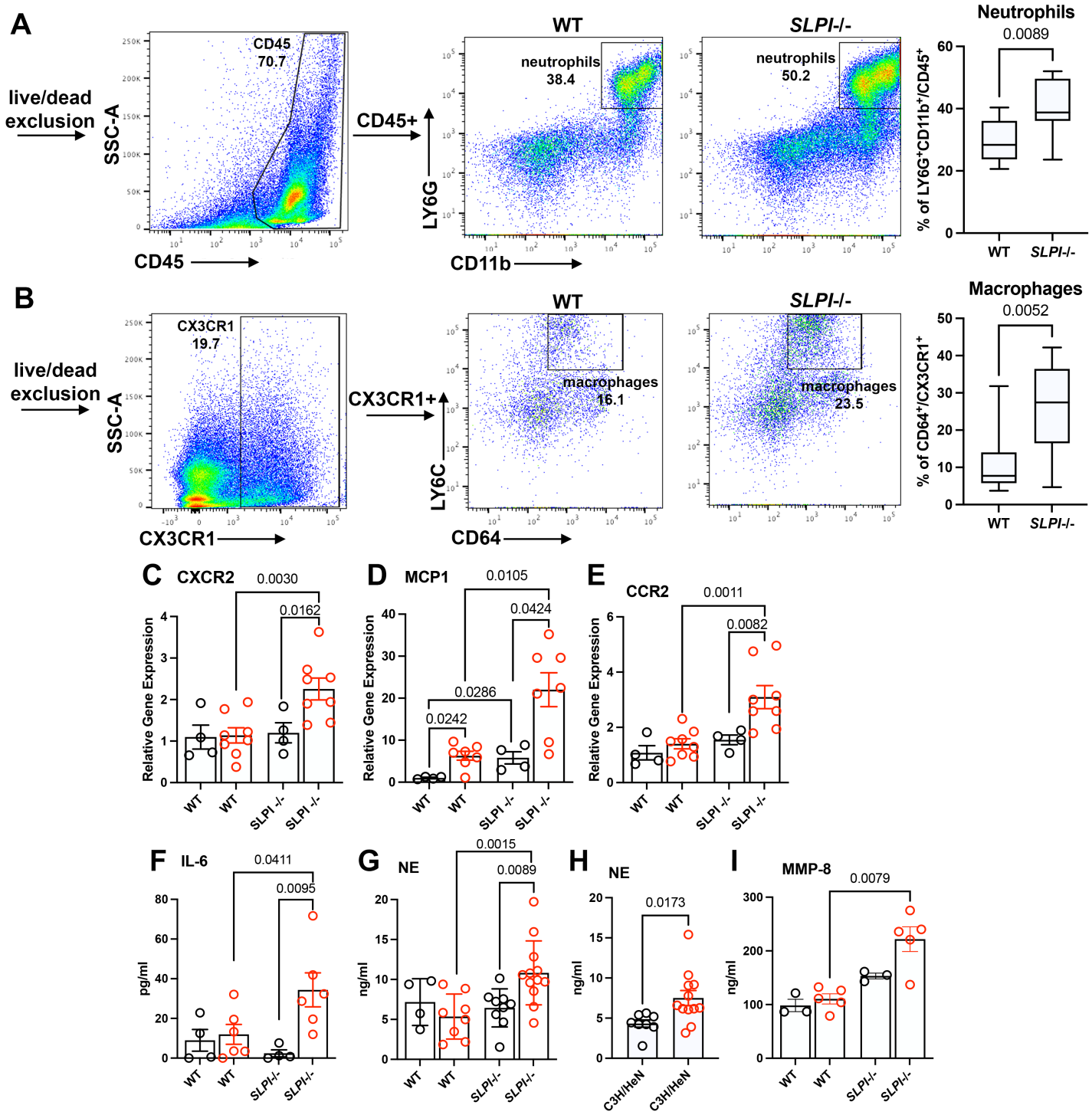
A
live/dead exclusion
SSC-A
CD45
CD45 70.7
CD45+
LY6G
CD11b
WT
SLPI-/-
neutrophils 38.4
neutrophils 50.2
Neutrophils
0.0089
% of LY6G+CD11b+/CD45+
B
live/dead exclusion
SSC-A
CX3CR1
CX3CR1 19.7
CX3CR1+
LY6C
CD64
macrophages 16.1
macrophages 23.5
Macrophages
0.0052
% of CD64+/CX3CR1+
C CXCR2
0.0030
0.0162
D MCP1
0.0105
0.0424
0.0286
0.0242
E CCR2
0.0011
0.0082
Relative Gene Expression
WT
SLPI -/-
F IL-6
0.0411
0.0095
pg/ml
G NE
0.0015
0.0089
ng/ml
H NE
0.0173
C3H/HeN
I MMP-8
0.0079
SLPI-/-

Figure 4

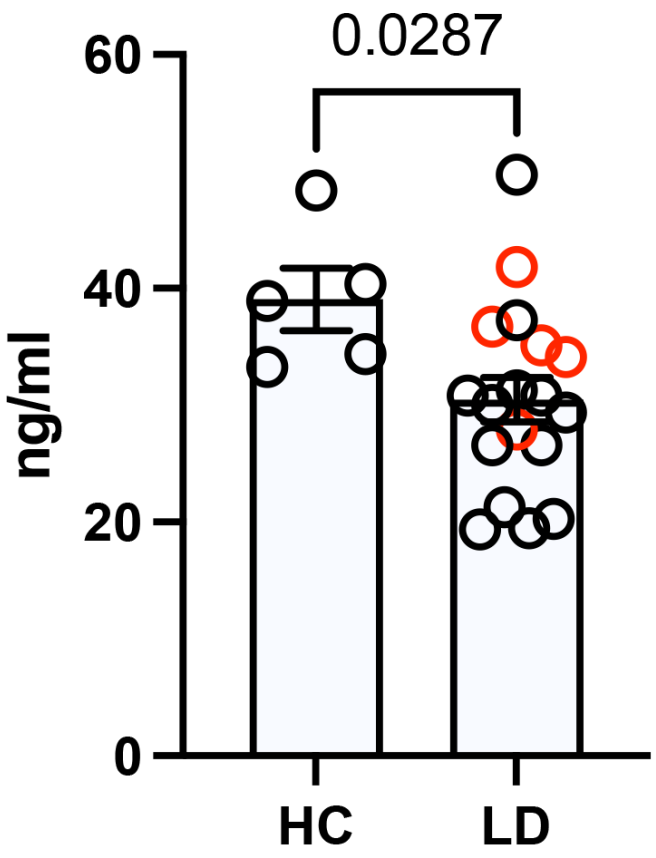

Figure 5

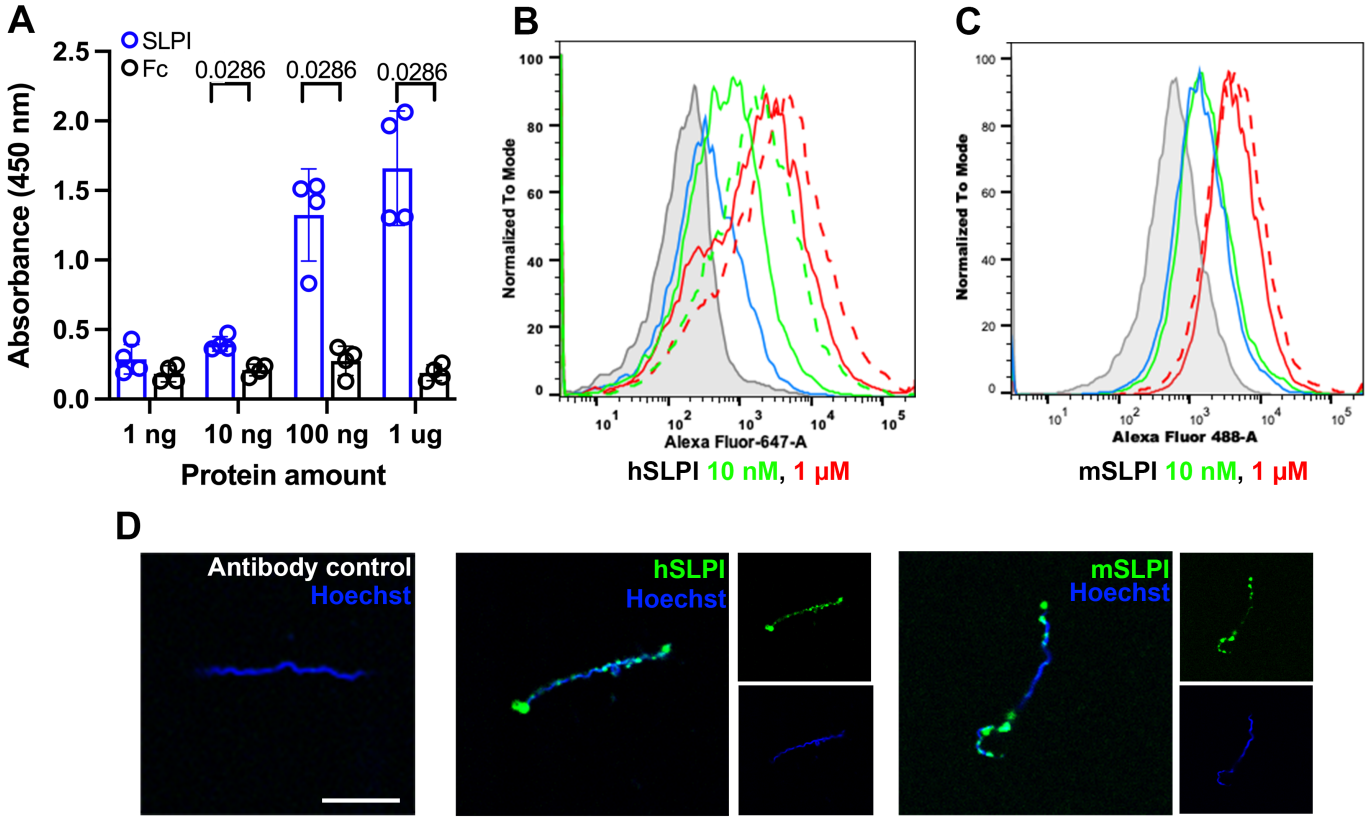
A
SLPI
Fc
0.0286
0.0286
0.0286
Absorbance (450 nm)
2.5
2.0
1.5
1.0
0.5
0.0
1 ng
10 ng
100 ng
1 ug
Protein amount
B
Normalized To Mode
Alexa Fluor-647-A
hSLPI 10 nM, 1 μM
C
Normalized To Mode
Alexa Fluor 488-A
mSLPI 10 nM, 1 μM
D
Antibody control
Hoechst
hSLPI
Hoechst
mSLPI
Hoechst